Paper Plane Aerodynamic Objects Case Study

Bill Crowther, 25th August 2024

bill.crowther@manchester.ac.uk

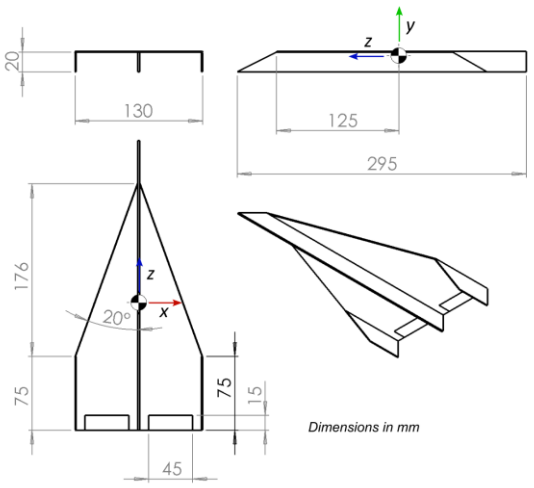

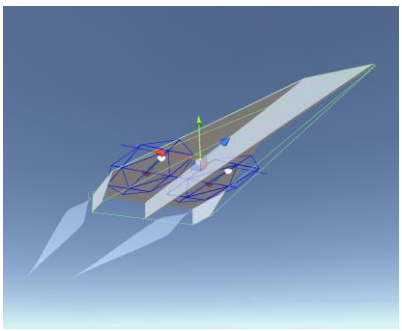

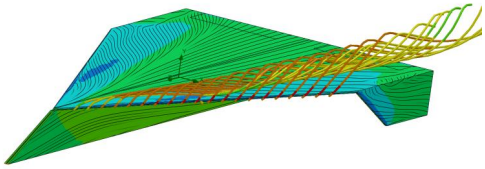

Objective

Model a paper plane using AO2

Introduction

Paper aeroplanes are typically based on a low aspect ratio cropped delta wing planform due to the constraints of the rigidity of the paper and the folded construction method. Paper aeroplanes are also flying wing or *tailless* configurations which means that setting up for successful flight dynamics is a bit more complex than for aircraft with a separate tail. This is because on a tailless aircraft aerodynamic control surfaces on the wing trailing edge have to be used for both longitudinal balance (adjustment of trim angle of attack, which sets airspeed in steady gliding flight) and for lateral control (adjustment of the lateral lift distribution, which controls roll rate and hence rate of turn if the aircraft is directionally stable). Control of trim angle of attack is via the change in pitching moment generated by control deflection, whereas control of lateral lift distribution is via the change in local lift due to control deflection. A fundamental challenge with getting good aerodynamic performance out of tailless aircraft is that to balance the aircraft in flight so that it is produces positive lift, trailing edge controls need to be deflected trailing edge up to produce a positive (nose up) pitching moment. However, this control action *decreases* the local lift on the surface, which is the opposite effect to what is needed. The solution is to ensure that the aircraft is only modestly stable in pitch so that a given

change in control deflection produces a large change in trim angle of attack for only a relatively small decrement in local lift.

Geometric definition

The geometric definition of the 'Delta Dart' paper aeroplane used for this case study is shown in Figure 1 based on an example that is known to work well in practice. The aircraft folded from a single sheet of A4 paper. The centre of mass placement shown is based on the natural location obtained by folding (no ballast added to move the location). The aircraft has folded-down wing tip fins mainly for structural reasons as these folds increase the rigidity of the outer wing and hence make repeatable flight more achievable. The centre fuselage has been made parallel and its depth is the same as the wing tips. Altering the fuselage geometry changes both the overall aircraft geometry and the centre of mass location. The leading edge sweep of the wing is 70 degrees (zero degrees = unswept). The wing planform area is 0.02m^2 and the span is 0.13m giving an aspect ratio of 0.86. The mean aerodynamic chord (mac) found from geometry is 0.21m in length and located at 41% semi span. The predicted aerodynamic centre location using the quarter chord of the mac is approximately 125mm aft of the leading edge (this happens to be coincident with the centre of mass location). Two trailing edge controls are implemented in the form of constant chord flaps (flap chord 7% of mac).

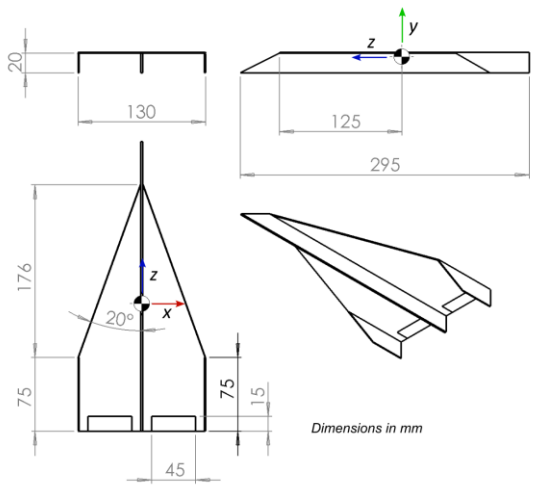

Figure 1 Delta dart geometry

The overall mass is 5g and the inertia leading diagonal (from CAD) is I_{xx}=2.6e-5, I_{yy}=3.0e-5, I_{zz}=5e-6 kg m^2 using the coordinate system shown in Figure 1.

Baseline Aerodynamics

CFD set up

A Computational Fluid Dynamics analysis of the delta dart was performed using Solidworks FlowSimulation. A cartesian mesh with the order of around 1 million cells was used, Figure 2. Mesh control planes were used to increase cell count within the approximate bounding box of

the model geometry. For longitudinal studies the model used symmetry about the yz plane. For sideslip studies a full model was used. Improved resolution of the leading edges was obtained using curvature based refinement of the basic mesh. Aerodynamic attitude was varied by varying the free stream wind vector (model meshing remained constant). A steady laminar and turbulent solver was used. Package default values were used for the convergence criteria. The moment reference point was the centre of mass location as identified in Figure 1. Moveable control surfaces were implemented with deflection angle settable within the CFD experiment control manager.

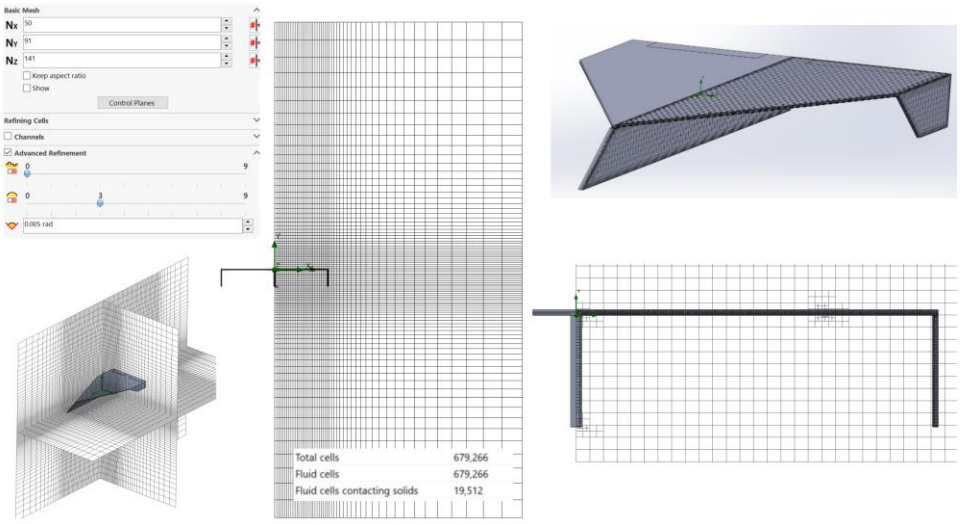

Figure 2 CFD meshing

CFD results and comparison with theory

Example CFD visualisation output is shown in Figure 3 for a typical cruise angle of attack of 7 degrees (zero sideslip). A well defined leading edge vortex dominates the upper flowfield of the wing, with clear signature of vortex induced flow in the surface streamlines and signature of vortex suction in the surface pressure contours.

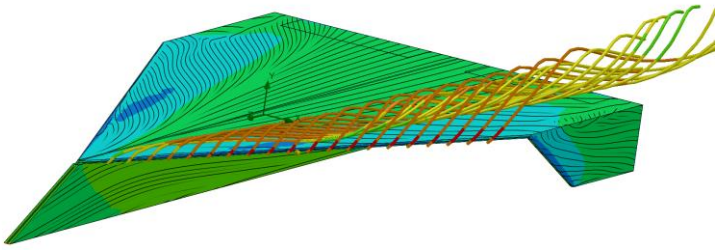

Figure 3 Aerodynamics at 7 degrees angle of attack, surface streamlines, surface pressure contours, leading edge vortex path lines shown on port wing.

Force and moment data for an alpha sweep between approximately -5 and +55 degrees angle of attack is shown in Figure 4. At low angles of attack, the wing lift curve slope is approximately equivalent to that of the theoretical value predicted using the given aspect ratio of 0.86 and lifting line theory (a=2pi AR/(2+AR). At higher angles of attack the lift curve is steeper, with the

increase normally explained by the presence of vortex lift. Here, a theoretical lift curve based on an aspect ratio of 2 is a closer fit to the data. Pitching moment data shows a stable response with lift coefficient (DCM/DCL is negative). A theoretical pitching moment curves for a static margin of 0.1 and 0.05 are shown for comparison. The slope at low alpha is consistent with a static margin of 0.05 whereas at higher angles of attack the model with a static margin of 0.1 is a better fit. Note that the pitching moment coefficient C_M is defined using the standard aerospace coordinate system such that positive pitching moments are nose up. The lift to drag ratio as a function of lift coefficient is shown in Figure 4c. From CFD, the best L/D is around 4.2 and this is achieved at a lift coefficient of around 0.3. The theoretical model for L/D is based on a drag polar using a Cdo of 0.03 from CFD data, and aspect ratio of 0.86 given from geometry and a planform efficiency factor k of 1.3 calibrated to give the best fit to the data. Use of a k value of 1 increases the peak theoretical L/D from around 4.1 to around 4.7.

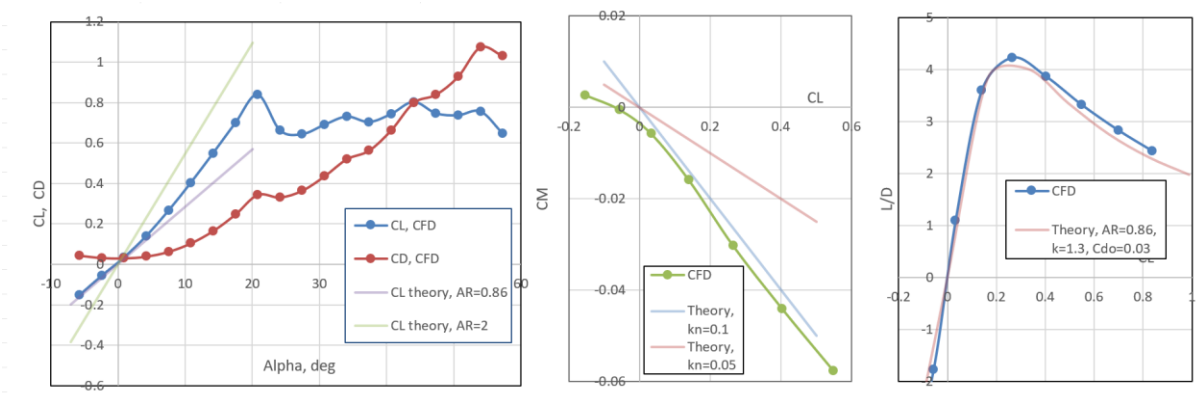

Figure 4 Aerodynamic force and moments with angle of attack, CFD with comparison with theory

The effect of changing elevon deflection on the pitching moment with lift coefficient curves is shown in Figure 5. Negative deflection of the elevons (trailing edge up) gives a positive increment in pitching moment at zero lift (CM_o) consistent with expectations for the effect of camber from thin aerofoil theory. The slope of the curves remains largely unaffected, as would be expected. The trim points (marked with stars) for the different elevon deflections show that the given elevons could trim the aircraft over a useful range of lift coefficients, with the best glide performance (best L/D, occurring at CL~0.3) achieved with an elevon defection somewhere between -5 and -10 degrees.

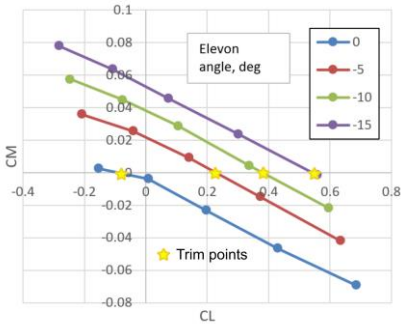

Figure 5 Effect of elevon deflection on CM-CL curves, CFD. Negative elevon deflection = trailing edge up.

The secondary effects of elevon deflection in terms of lift magnitude at a given angle of attack and L/D profile are shown in Figure 6. Deflection of the elevons trailing edge up creates a negative offset in the lift meaning that the angle of attack would have to be increased to achieve

the same lift. The effect on aerodynamic performance shown in the L/D curves shows that for a 15 degree elevon deflection the best L/D is reduced from 4 to 3. This reinforces the need to use relaxed levels of stability for tailless aircraft so that trim can be achieved with minimal control effort and hence minimum reduction in performance due to control secondary effects.

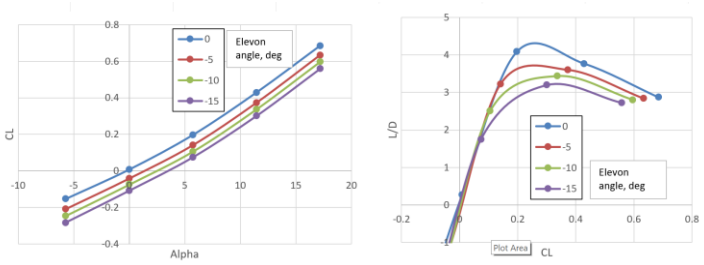

Figure 6 Secondary aerodynamic effects of elevon deflection, CFD

The lateral aerodynamic behaviour at a lift coefficient of 0.3 (best L/D) is shown in Figure 7, where Beta (sideslip angle), Croll, Cyaw and CM are defined using standard aerospace conventions. For positive sideslip (wind coming from starboard), the rolling moment is -ve (starboard wing up) and the yawing moment is +ve (nose swings to starboard) consistent with expectations for positive lateral stability.

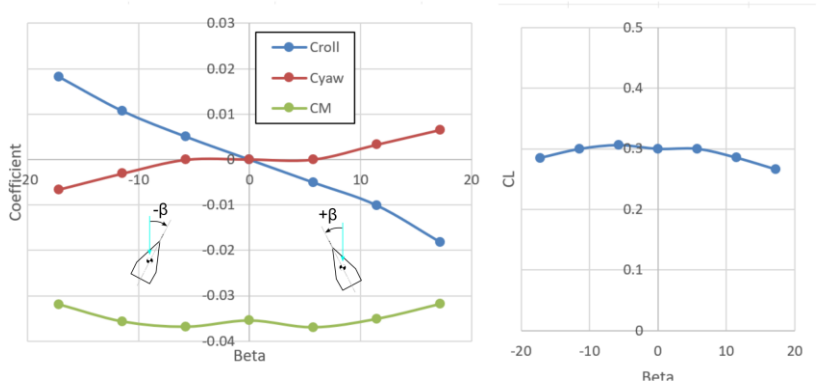

Figure 7 Effect of sideslip at 8 degrees angle of attack, CFD

Aerodynamic Objects set up

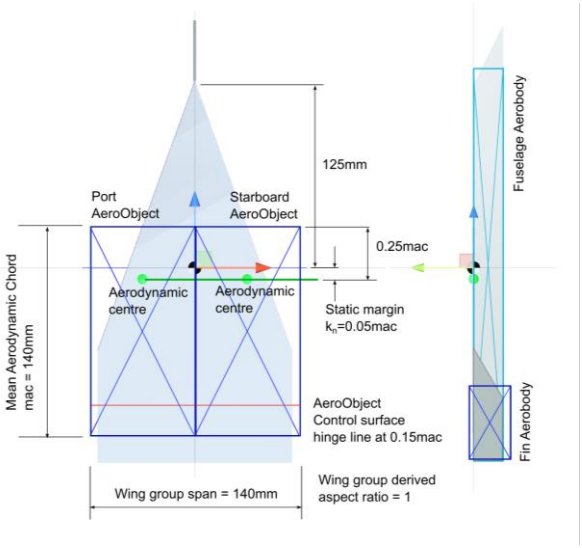

Figure 8 Delta dart AeroObject set up

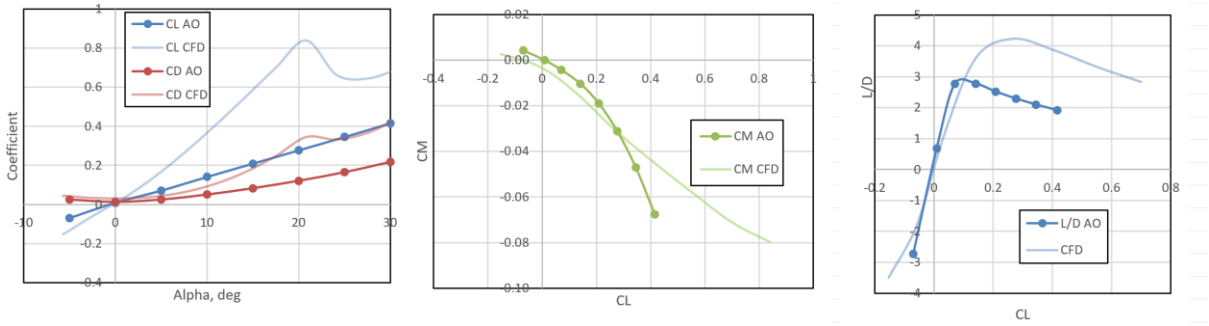

Figure 9 Aero force and moment data from AO/Unity

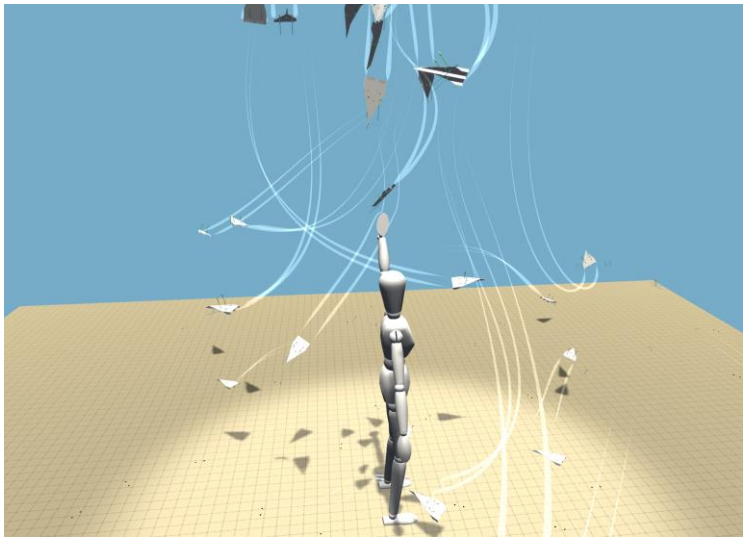

Figure 10 Paper plane demo

Conclusion

The aerodynamics of paper aeroplanes has been investigated from a theoretical and analytical point of view and a usefully representative aerodynamic model has been successfully set up in Aerodynamic Objects using a block element approach.

For the case study aircraft, the best lift drag ratio achieved was around 4 and this occurred at a lift coefficient of around 0.3. From CFD, stall occurs around 20 degrees angle of attack and CLmax was around 0.8. With uncorrected aspect ratio, the AO model predicted a lift coefficient of 0.4 for the same angle of attack

The effect of leading edge separation on swept wings is currently not modelled in AO and hence AO models underpredict lift at higher lift coefficients up to stall. This can be corrected in a simply way by increasing the modelled aspect ratio, or by implementing a swept leading edge correction term.